HHS Public Access

Author manuscript

Proc SPIE Int Soc Opt Eng. Author manuscript; available in PMC 2015 January 22.

Published in final edited form as:

Proc SPIE Int Soc Opt Eng. 2013 September 20; 8815: . doi:10.1117/12.2027253.

In vivo photoacoustic imaging of breast cancer tumor with HER2-targeted nanodiamonds

Ti Zhang[a], **Huizhong Cui**[b], **Chia-Yi Fang**[c], **Janggun Jo**[b], **Xinmai Yang**[b], **Huan-Cheng Chang**[c], and **M. Laird Forrest**[*,a]

[a]Department of Pharmaceutical Chemistry, The University of Kansas, Lawrence, KS USA 66045

[b]Department of Mechanical Engineering, Bioengineering Research Center, The University of Kansas, Lawrence, KS USA 66045

[c]Institute of Atomic and Molecular Science, Academia Sinica, Taipei, Taiwan 10617

Abstract

Radiation-damaged nanodiamonds (NDs) are ideal optical contrast agents for photoacoustic (PA) imaging in biological tissues due to their good biocompatibility and high optical absorbance in the near-infrared (NIR) range. Acid treated NDs are oxidized to form carboxyl groups on the surface, functionalized with polyethylene glycol (PEG) and human epidermal growth factor receptor 2 (HER2) targeting ligand for breast cancer tumor imaging. Because of the specific binding of the ligand conjugated NDs to the HER2-overexpressing murine breast cancer cells (4T1.2 neu), the tumor tissues are significantly delineated from the surrounding normal tissue at wavelength of 820 nm under the PA imaging modality. Moreover, HER2 targeted NDs (HER2-PEG-NDs) result in higher accumulation in HER2 positive breast tumors as compared to non-targeted NDs after intravenous injection (i.v.). Longer retention time of HER-PEG-NDs is observed in HER2 overexpressing tumor model than that in negative tumor model (4T1.2). This demonstrates that targeting moiety conjugated NDs have great potential for the sensitive detection of cancer tumors and provide an attractive delivery strategy for anti-cancer drugs.

Keywords

Nanodiamond; Photoacoustic Imaging; Breast Cancer; HER2

1. INTRODUCTION

Detection of cancerous tumor at an early stage is critical to diagnose cancer accurately, initiate treatment effectively, and thus improve patients' survival.[1, 2] Traditional biomedical imaging modalities, such as computed tomography (CT) and ultrasound, have been used to visualize tumors in the clinic.[3–5] However, these techniques suffer from their intrinsic disadvantages, such as the relatively low spatial resolution, specificity and contrast, which limit their application for providing sufficient functional and molecular information of imaging areas. Although the resolution could reach as high as several micrometers with the

[*]mforrest@ku.edu; phone 1 785 864-4388; fax 1 785 864-4388.

development of optical imaging techniques, the high optical scattering of biological tissues limits their imaging depth to less than a few millimeters, and consequently impedes their further in vivo applications. For example, optical fluorescence imaging is capable of providing specific molecular information at subcellular resolution, however, this technique only allows the imaging at a depth of 1–2 mm.[6, 7]

Photoacoustic (PA) imaging is an emerging non-invasive and non-ionizing biomedical imaging modality combining a high spatial resolution of ultrasound technique and excellent contrast of optical imaging with the help of various contrast agents.[8–10] Within the photoacoustic effect, light is absorbed by either the tissue or exogenous agent in the interested tissue and converted to ultrasound via its transient thermal elastic expansion. Because acoustic attenuation is 1000 times weaker than that of pure optical imaging when traveling in the biological tissue, PA imaging has a great penetration depth up to several centimeters with reasonable resolution.[11, 12] PA imaging is an absorption-based technique so that the biological tissue components having high optical absorbance, such as hemoglobin and melanin, which can be used as endogenous contrast agents to image blood vessels, hemoglobin oxygenation and tumor angiogenesis.[13–16] Without the assistance of exogenous contrast agents, PA imaging has shown to be useful in various applications, but cancer tumors except melanoma are always transparent and do not absorb light much so differently from surrounding normal tissues. The introduction of exogenous contrast agents has greatly enhanced imaging sensitivity and specificity.[17] Organic dyes, quantum dots (QDs) and plasmonic nanoparticles have been widely used in the PA imaging. Among these, contrast agents having high optical absorbance in the near-infrared (NIR) region are more attractive since the PA signal contribution from normal tissue and hemoglobin is minimum and Mie scattering effect is relatively weak within the optical window at the wavelength of 700 to 1100 nm. In addition to the strong absorption in the NIR range, other properties of contrast agents must be considered for the biomedical applications, such as toxicity, size, stability and surface chemistry. Some biocompatible dyes, including methylene blue and indocyanine green, have been used in PA imaging system. However, organic dyes are so small molecules as to be cleared quickly from body through the renal system, and fluorescence suffers from the intermittency and photobleaching which limits their further application even though their conjugation to nanoparticles makes them have suitable size for passive tumor uptake. The most developed PA contrast agents are plamonic nanoparticles due to their tunable and five times stronger optical absorption than dyes based on the surface plasmon resonance (SPR) effect. Gold nanorods are extensively used in PA imaging because of its relatively simple synthesis, even stronger plasmon resonance absorption in the NIR range.[18] The great advances in surface functionalization encourage its use in tumor imaging.[19] However, gold nanorods tend to melt and thus deform under strong and longer laser light irradation. Although this strategy has been used to release the DNA oligonucleotides, nanoparticles were not able to provide consistant PA signals at a specific wavelength during the whole imaging process.[20, 21] In addition, long-term toxicity of gold nanoparticles has to be considered in further applications in clinic.

Owing to the excellent biocompatibility and exceptional optical stability, nanodiamonds (NDs) are shown to be outstanding optical contrast agent and drug carriers for biomedical applications.[22] By introducing nitrogen vacancy center as a fluorophor in the NDs,

fluorescent nanodiamonds (FNDs) exhibit competitive advantages over organic fluorescent dyes and quantum dots (QDs) due to the long-term stability and non-toxicity as an in vivo contrast agent.[23–25] Recently, alternative strategy for using nanodiamonds as imaging contrast agents have also been reported. Making use of the detectable electron spin resonance of nitrogen-vacancy centers, different shapes of nanodiamond targets within the chicken breast tissues were imaged with a spatial resolution of ~800 μm.[26] Carbon-dots (CDs) with tunable and strong photoluminescence produced by hydrothermal oxidation of nanodiamonds have been utilized for cell imaging.[27] Fabrication of nanodiamonds with diethylenetriaminepentaacetic acid (DTPA) - Gd chelate improved the signal intensity on T1-weighted magnetic resonance images.[28] Non-fluorescent nanodiamonds with ~70 nm in diameter employed as a PA imaging agent was firstly proposed in our earlier publication.[29] Since a low fluorescence quantum yield results in more efficient PA signal generation, nanodiamonds shown ~70 times stronger PA signals than gold nanorods on a particle molar basis.

In this work, we are aiming at diagnosing early stage breast cancer using 35 nm radiation-damaged nanodiamonds. To enhance the systemic circulation time and particle stability, nanodiamonds were firstly surface functionalized with polyethylene glycol (PEG). To further enhance the imaging sensitivity and contrast of tumor areas, PEGylated NDs were then conjugated to anti-human epidermal growth factor receptor 2 (HER2) targeting peptide, KCCSYL.

This six-amino-acid KCCYSL sequence was identified in HER2-positive breast cancer cells and exhibited 295 nmol/L affinity to HER2 receptor which enabled its great potential in tumor-imaging application.[30, 31]

2. METHODOLOGY

2.1 Materials and chemicals

N-(3-Dimethylaminopropyl)-N′-ethylcarbodiimide hydrochloride (EDC·HCl), N-Hydroxysuccinimide (NHS), sodium borate, sodium hydroxide, potassium chloride (KCl) were purchased from Sigma-Aldrich (St. Louis, MO). Amine-PEG2000-amine was purchased from Jenkem Technology (Allen, TX). Fetal bovine serum (FBS) was purchased from Fisher Scientific (Pittsbrugh, PA). Dulbecco's Modified Eagle's Medium (DMEM) was purchased from Lonza (Allendale, NJ). Anti-Human epidermal growth factor receptor 2 (anti-HER2) peptide (KCCYSL) was provided by Dr. Kun Cheng (University of Missouri-Kansas City, MO). 4T1.2 breast cancer cells were provided by Beth A. Vorderstrasse (Washington State University, WA) and used with the permission of Robin Anderson (Peter MacCallum Cancer Centre, East Melbourne, Australia). Deionized (DI) water was used for preparing all of the solutions.

2.2 Bioconjugation and characterization

Nanodiamonds were synthesized as we described before.[19] The conjugation of amine-PEG-amine and anti-HER2 peptide with NDs followed a standard EDC/NHS-mediated coupling procedure.[36, 37] Briefly, 2 mg of NDs were dissolved in 2 mL of sodium borate buffer (10 mM, pH 8.5), followed by sonication for 30 min. EDC·HCl (4 mg) and NHS (4 mg) were

added to the NDs solution, which was stirred at room temperature for 0.5 hr to form the amine-reactive NDs intermediates. A 0.5 mL solution of amine-PEG2000-amine (10 mg) was finally added to the above solution. After stirring overnight, the amine-PEG-NDs were purified by centrifugation at 10,000 × g for 5 min, and particle precipitate was washed three times with DI water. To synthesize the HER2-PEG-NDs, the carboxyl terminus of anti-HER2 peptide (1 mg) was pre-activated by mixing with EDC·HCl (4 mg) and NHS (4 mg) for 0.5 hr in DI water, followed by the addition of amine-PEG-NDs (2 mg) aqueous solution. As a result, the anti-HER2 peptide was covalently linked to the PEGylated NDs after stirring the mixture overnight. The resulting nanoparticles were separated from the solution by centrifugation, washed with DI water three times, and dried in SpeedVap (Labconco).

Fourier-transform infrared spectroscopy (IRAffinity-1 FTIR Spectrophotometer, Shimazu) was conducted to confirm the coating of PEG and anti-HER2 peptide on the NDs. Hydrodynamic diameters and zeta potentials of ND particles in aqueous solution were determined using ZetaPALS (Brookhaven Instrument Corporation). All measurements were carried out in five replicates. The morphology of NDs was determined using high-resolution Transmission Electron Microscope (TEM) (FEI Tecnai F20 XT Field Emission TEM), and sample was applied on a lacey carbon coated copper grid (TED PELLA).

The optical characterization of the NDs was measured using a same setup as our former paper.[29] DI water suspension of NDs was injected into Tygon tubing (1 mm ID, 1.78 mm OD), which was immersed in the water. The PA amplitude of NDs at different wavelengths was recorded with 5 replicates.

2.3 Cell culture and cellular uptake

4T1.2 and 4T1.2 neu breast cancer cells were cultured in DMEM containing 10% FBS and 1% L-glutamine at 37 °C supplied with 5% CO_2 under a humidified environment.

Cells were seeded onto a 12-well culture plate, in which poly L-Lysine precoated glass coverslips (BD, Franklin Lakes, NJ) were placed previously, at a density of 50,000 cells per well for overnight. 4T1.2 neu cells were treated with or without 32 μg (based on NDs) PEG-NDs or HER2-PEG-NDs, whereas 4T1.2 cells were treated with or without 32 μg (based on NDs) HER2-PEG-NDs followed by incubation at 37 °C for 4 hr. Then the cells were washed three times with 3 mL PBS solution and imaged using inverted microscope (Eclipse TE2000-U, Nikon).

2.4 Photoacoustic imaging

The experimental setup for PA imaging of biological tissues is shown in Scheme 1. The deep reflection-mode PA imaging system is capable of sub 0.2-mm resolution at depths of 19 mm and penetration of up to 38 mm.[38] In this study we used a same configuration as described previously.[39] A 532-nm Q-switched Nd:YAG laser (Surelite III, Continuum) was employed to pump an optical parametric oscillator laser (Surelite OPO PLUS, Continuum) with 6-ns pulses and repetition rate of 10 Hz. The laser output was transformed through an optical condenser to a ring-shape illumination, which is confocal with ultrasonic transducer in the targeted area. The illumination beam had a diameter of 7 mm on the tissue surface,

and the laser fluence was 18 mJ cm^{-2}, which was lower than laser safety limits (20 mJ cm^{-2}) recommended by the American National Standards Institute (ANSI). A 5-MHz transducer (35-mm focal length; 70% -6-dB fractional bandwidth, SU-108-013, Sonic Concepts) was used to collect the photoacoustic signals, which were amplified by a pre-amplifier (5072PR, Olympus-NDT) and then collected by a PC through an A/D Scope Card (CS21G8-256MS, Gage) with a 125-MHz sampling rate for analyzing and forming PA images. Female BALB/c mice were used in the experiments in accordance with the guide and supervision of the Institutional Animal Care and Use Committee at University of Kansas. The murine breast cancer cells, 4T1.2 and 4T1.2 neu, were prepared in PBS solution at a concentration of 2×10^7 cells/mL, and kept in ice bath before injection. Mice were under anesthesia with 1.5% isoflurane in 1:1 oxygen-air mixture. 50 μL cell suspension was injected subcutaneously into the right mammary fat pad under the nipple of the mice using 30-ga needles. Mice were ready for PA imaging when the breast cancer tumors had a size of ~5 × 5 mm.

Before each imaging experiment, the animals were anesthetized with a mixture of ketamine (87 mg/kg body weight) and xylazine (13 mg/kg body weight). The right breast areas of mice were shaved using standard surgical hair removal lotion to avoid the interference from hairs to ultrasound propagation. The mice were maintained under anesthesia on a warm pad, and underneath the membrane in the center of the bottom of the water tank during the entire imaging process. Between the mouse skin and the membrane, ultrasound gel was applied and served as coupling medium. Breath of mice was visually monitored and maintained at one breath per two seconds. The PA images of the breast tumor areas were obtained as background images before injecting PEG-NDs or HER2-PEG-NDs particles. Once the imaging depth (2 – 3 mm) was determined along with the imaging resolution of ~270 μm, particles were intravenously administrated into the mice tail vein. The tumor areas were scanned continuously and repeatedly by PA system at a laser wavelength of 820 nm.

3. RESULTS AND DISCUSSION

3.1 Synthesis and characterization

In order to verify the successful conjugation of amine-PEG-amine (MW 2000) and anti-HER2 targeting peptide to the NDs via EDC/NHS mediated reactions, FTIR spectra were collected at the end of each step, as shown in Figure 1. The appearance of the characteristic peaks, at 1250 and 1035 cm^{-1}, of the PEG confirmed the presence of the coating on the surface of bare NDs. In addition, the FTIR spectrum of HER2-PEG-NDs displays same intense peaks as anti-HER2 peptide at 1656 and 1521 cm^{-1} corresponding to the stretching vibration of the amino group on lysine and hydroxyl group on tyrosine, respectively. The band at 1200–1260 cm^{-1} resulted from the -OH stretching vibration in the serine. These data confirmed the introduction of HER2 targeting peptide onto the NDs with the linkage of amine-PEG-amime. ~10% of the carboxyl groups on the NDs are reacted with amine-PEG-amine, which is assumed similarly as we described before, and then are conjugated with anti-HER2 peptide in a 1:1:1 ratio. Yield for the amount of targeting peptide on the surface of NDs could be estimated as the order of ~10^{-5} mol g^{-1}.

3.2 Morphology and optical properties

In addition to the FTIR, the coating of PEG and HER2 targeting peptide was further confirmed by the hydrodynamic diameters and zeta potentials of the NDs and the surface-functionalized NDs. Table 1 shows the progressive increase in particle sizes and change in charge state of the nanoparticle surfaces. The size distribution of nanoparticles was plotted in Figure 2. The decrease in the negative charges was due to the introduction of amino groups from amine-PEG-amino and lysine residues in anti-HER2 peptides.

The optical absorption characteristic of NDs was plotted as a function of wavelength using UV-Vis spectrometer (Figure 3a). The absorption intensity decreased 80% from 450 nm to 850 nm. Since photoacoustic imaging is an absorption-based technology, the PA signal amplitude decreased in proportion to the decline of the optical absorption in the tunable wavelength range of PA imaging system. Although the small bump at 720 nm in the photoacoustic spectrum is not shown in the UV-Vis absorption spectrum, the signal intensity dropped 50% from 700 nm to 840 nm, which had the same tendency as that in absorption spectrum.

3.3 Cellular imaging

The targeting ability of anti-HER2 peptide was validated *in vitro* by the brightfield images of HER2 receptor positive and negative breast cancer cells (4T1.2 neu and 4T1.2 cells) (Figure 4). As negative controls, 4T1.2 neu breast cancer cells were treated with non-targeting PEGylated NDs (4T1.2 neu cells + PEG-NDs) and HER2 negative 4T1.2 cells were treated with targeting PEGylated NDs (4T1.2 cells + HER2-PEG-NDs). The clusters of ND particles present black spots in the cells. There was no obvious accumulations of NDs in the control groups after 4-hr incubation (Figure 4b and 4d), whereas a large amount of HER2-PEG-NDs were found in the HER2 overexpressing cells (Figure 4e). Moreover, some particle clusters were detected in the cell membranes (arrows in the Figure 4), which is not seen in Figure 4b and 4d. The phenomenon demonstrates that HER2-PEG-NDs effectively bound to the HER2 receptors on the cell membrane and entered cells via receptor-mediated endocytosis.

3.4 *In vivo* PA imaging

The tumor areas of mice bearing breast cancer were imaged under PA imaging system at 820 nm. Although NDs had stronger absorption and thus higher contrast against background tissues at 700 nm comparing to 820 nm, the signal contributions from blood vessel would be also greater. Herein, imaging wavelength of 820 nm was chosen because the absorption of hemoglobin and Mie scattering is minimized and the PA signal enhancement is more specifically in the pictures due to the accumulation of ND particles. Prior to the injection, a region of interest (ROI) was selected on the right side of the breast and defined as background (BG). Imaging depths were adjusted so as to obtain the best spatial resolution.

BALB/C mice were injected with identical amount of diamond nanoparticles (35 μg on the NDs basis) via tail veins. Once the imaging depth is determined, PA images of same areas were taken continually with 1-hr intervals and processed to remove the signals from mouse skin as illustrated in Figure 5. Of the two control groups, one is HER2 positive tumor model

(4T1.2 neu) treated with PEG-NDs (Figure 5a), and the other one is HER2 negative tumor model (4T1.2) treated with HER2-PEG-DNDs (Figure 5b). In the PA images, the blood vessels (BVs) were highlighted because of the relatively higher optical absorption of hemoglobin over normal optical transparent tissues. Beginning at 2nd hour post-injection, the blood contrast was enhanced as indicated by the colorbars in the figures, and signal intensity reached maximum at the 6th, 4th and 5th hour scanning session of each group. Moreover, owing to the enhanced permeability and retention effect, nanoparticles tend to leak out from the abnormal vasculature and accumulate in the solid tumor. However, Li M.L. *etc* demonstrated that gold nanoshells could not actually enter the necrotic tissues of tumor, but accumulated within the tumor cortex and delineated the tumor contour when the nanoshells were detected by PA microscopy under the wavelength of 800nm.[33] NDs particles progressively migrated from blood vessels toward tumor region and were uptaken within breast cancer tumor surface, which was also observed in our PA images. Compared to the control groups, HER2 positive breast cancer model treated with HER2-PEG-NDs intravenously had higher signal enhancement around the tumor region and finally delineate the entire tumor (dashed circle in Figure 5c) at the 8th hour. The presence of NDs within the tumor core was not effectively detected because of both the necrotic feature and high interstitial pressure of tumor cores.[34] In addition, no observation of NDs on the top surface of the tumor may be explained by the pressure from water tank above the tumor area hindering the particle accumulation. Meanwhile, slight accumulation of nanodiamonds appeared in the control groups make it difficult to differentiate the tumor regions without the illustration of photographs of ROI. These phenomena demonstrate that the tumor uptake of HER2-PEG-NDs is indeed a target-specific event. This result is further confirmed by the prolonged retention time within tumors in the HER2 targeting treatment group. The signal intensity of tumor region was monitored and compared between two consecutive scanning until the decrease in signal amplitude was acquired. As shown in Figure 5d, the signal decrease was found after the 8th hour on average in Group 3, whereas in Group 1 and 2, the T_{max} at ~ 6th hour is significantly shorter than Group 3 ($p < 0.05$, $n = 3$). The longer tumor retention time indicates that high HER2-receptor targeting specificity of HER2-PEG-NDs greatly avoid uptake by the RES and clearance by blood circulation in contrast to non-targeted NDs.[35]

4. CONCLUSIONS

While tons of PA contrast agents for cancerous tumor detection have been proposed, it is still facing some problems concerning light stability and long-term toxicity. In this work, non-toxic, stable and tageting moiety modified non-fluorescent nanodiamonds were successfully developed as a novel *in vivo* photoacoustic imaging contrast agent and shown to facilitate the optical contrast enhancement of breast cancerous tumor contour for effective HER2 positive breast cancer diagnosis. The conjugation of anti-HER2 peptide with PEGylated NDs was observed to lead to an enhancement in the internalization by HER2 overexpressing tumor cells (4T1.2 neu) and longer residence time in the tumor region. The long-term biocompatibility study of the nanodiamonds after intraperitoneal injection have been performed for 12 weeks and repored in our earlier publication, which indicated that the NDs administration did not result in any apparent toxicological effects.[24] We expect this

targeting-nanodiamond-PA imaging platform to provide a new oppotunity for sensitive detection of cancer tumors and become a promising delivery strategy for anti-cancer drugs.

Acknowledgments

This work was funded in part by the National Institutes of Health (1R01CA173292-01) and American Cancer Society (RSG-0813301CDD).

References

1. Ghosh SK, Uchida M, Yoo B, et al. Targeted imaging of breast tumor progression and therapeutic response in a human uMUC-1 expressing transgenic mouse model. International Journal of Cancer. 2013; 132(8):1860–1867.
2. Kaplan MA, Inal A, Kucukoner M, et al. Cranial Magnetic Resonance Imaging in the Staging of HER2-positive Breast Cancer Patients. Onkologie. 2013; 36(4):176–181. [PubMed: 23548965]
3. de la Zerda A, Bodapati S, Teed R, et al. Family of Enhanced Photoacoustic Imaging Agents for High-Sensitivity and Multiplexing Studies in Living Mice. Acs Nano. 2012; 6(6):4694–4701. [PubMed: 22607191]
4. Blick CGT, Nazir SA, Mallett S, et al. Evaluation of diagnostic strategies for bladder cancer using computed tomography (CT) urography, flexible cystoscopy and voided urine cytology: results for 778 patients from a hospital haematuria clinic. Bju International. 2012; 110(1):84–94. [PubMed: 22122739]
5. Salla C, Chatzipantelis P, Konstantinou P, et al. Endoscopic ultrasound-guided fine-needle aspiration cytology diagnosis of solid pseudopapillary tumor of the pancreas: A case report and literature review. World Journal of Gastroenterology. 2007; 13(38):5158–5163. [PubMed: 17876886]
6. Ntziachristos V, Bremer C, Weissleder R. Fluorescence imaging with near-infrared light: new technological advances that enable in vivo molecular imaging. European Radiology. 2003; 13(1): 195–208. [PubMed: 12541130]
7. Filonov GS, Krumholz A, Xia J, et al. Deep-Tissue Photoacoustic Tomography of a Genetically Encoded Near-Infrared Fluorescent Probe. Angewandte Chemie-International Edition. 2012; 51(6): 1448–1451.
8. Mallidi S, Luke GP, Emelianov S. Photoacoustic imaging in cancer detection, diagnosis, and treatment guidance. Trends in Biotechnology. 2011; 29(5):213–221. [PubMed: 21324541]
9. Yao JJ, Wang LHV. Photoacoustic tomography: fundamentals, advances and prospects. Contrast Media & Molecular Imaging. 2011; 6(5):332–345. [PubMed: 22025335]
10. de la Zerda A, Kim JW, Galanzha EI, et al. Advanced contrast nanoagents for photoacoustic molecular imaging, cytometry, blood test and photothermal theranostics. Contrast Media & Molecular Imaging. 2011; 6(5):346–369. [PubMed: 22025336]
11. Zhang HF, Maslov K, Stoica G, et al. Functional photoacoustic microscopy for high-resolution and noninvasive in vivo imaging. Nature Biotechnology. 2006; 24(7):848–851.
12. Wang LHV. Ultrasound-mediated biophotonic imaging: A review of acousto-optical tomography and photo-acoustic tomography. Disease Markers. 2003; 19(2–3):123–138. [PubMed: 15096709]
13. Hahn MA, Singh AK, Sharma P, et al. Nanoparticles as contrast agents for in-vivo bioimaging: current status and future perspectives. Analytical and Bioanalytical Chemistry. 2011; 399(1):3–27. [PubMed: 20924568]
14. Kolkman RGM, Hondebrink E, Steenbergen W, et al. Photoacoustic imaging of blood vessels with a double-ring sensor featuring a narrow angular aperture. Journal of Biomedical Optics. 2004; 9(6):1327–1335. [PubMed: 15568955]
15. Siphanto RI, Thumma KK, Kolkman RGM, et al. Serial noninvasive photoacoustic imaging of neovascularization in tumor angiogenesis. Optics Express. 2005; 13(1):89–95. [PubMed: 19488331]

16. Wang XD, Xie XY, Ku GN, et al. Noninvasive imaging of hemoglobin concentration and oxygenation in the rat brain using high-resolution photoacoustic tomography. Journal of Biomedical Optics. 2006; 11(2)
17. Cheng K, Cheng Z. Near Infrared Receptor-Targeted Nanoprobes for Early Diagnosis of Cancers. Current Medicinal Chemistry. 2012; 19(28):4767–4785. [PubMed: 22873665]
18. Nguyen Ngoc Long LVV, Kiem Chu Dinh, Doanh Sai Cong, Nguyet Cao Thi, Hang Pham Thi, Thien Nguyen Duy, Quynh Luu Manh. Synthesis and optical properties of colloidal gold nanoparticles. Journal of Physics: Conference Series. 2009; 187:9.
19. Huang P, Bao L, Zhang CL, et al. Folic acid-conjugated Silica-modified gold nanorods for X-ray/CT imaging-guided dual-mode radiation and photo-thermal therapy. Biomaterials. 2011; 32(36):9796–9809. [PubMed: 21917309]
20. Wijaya A, Schaffer SB, Pallares IG, et al. Selective Release of Multiple DNA Oligonucleotides from Gold Nanorods. Acs Nano. 2009; 3(1):80–86. [PubMed: 19206252]
21. Chen CC, Lin YP, Wang CW, et al. DNA-gold nanorod conjugates for remote control of localized gene expression by near infrared irradiation. Journal of the American Chemical Society. 2006; 128(11):3709–3715. [PubMed: 16536544]
22. Mochalin VN, Shenderova O, Ho D, et al. The properties and applications of nanodiamonds. Nature Nanotechnology. 2012; 7(1):11–23.
23. Chang YR, Lee HY, Chen K, et al. Mass production and dynamic imaging of fluorescent nanodiamonds. Nature Nanotechnology. 2008; 3(5):284–288.
24. Vaijayanthimala V, Cheng PY, Yeh SH, et al. The long-term stability and biocompatibility of fluorescent nanodiamond as an in vivo contrast agent. Biomaterials. 2012; 33(31):7794–7802. [PubMed: 22863379]
25. Vaijayanthimala V, Tzeng YK, Chang HC, et al. The biocompatibility of fluorescent nanodiamonds and their mechanism of cellular uptake. Nanotechnology. 2009; 20(42)
26. Hegyi A, Yablonovitch E. Molecular Imaging by Optically Detected Electron Spin Resonance of Nitrogen-Vacancies in Nanodiamonds. Nano Letters. 2013; 13(3):1173–1178. [PubMed: 23384363]
27. Zhang XY, Wang SQ, Zhu CY, et al. Carbon-dots derived from nanodiamond: Photoluminescence tunable nanoparticles for cell imaging. Journal of Colloid and Interface Science. 2013; 397:39–44. [PubMed: 23484769]
28. Nakamura T, Ohana T, Yabuno H, et al. Simple Fabrication of Gd(III)-DTPA-Nanodiamond Particles by Chemical Modification for Use as Magnetic Resonance Imaging (MRI) Contrast Agent. Applied Physics Express. 2013; 6(1)
29. Zhang T, Cui HZ, Fang CY, et al. Photoacoustic contrast imaging of biological tissues with nanodiamonds fabricated for high near-infrared absorbance. Journal of Biomedical Optics. 2013; 18(2)
30. Kumar SR, Quinn TP, Deutscher SL. Evaluation of an In-111-Radiolabeled peptide as a targeting and Imaging agent for ErbB-2 receptor-expressing breast carcinomas. Clinical Cancer Research. 2007; 13(20):6070–6079. [PubMed: 17947470]
31. Tai WY, Shukla RS, Qin B, et al. Development of a Peptide-Drug Conjugate for Prostate Cancer Therapy. Molecular Pharmaceutics. 2011; 8(3):901–912. [PubMed: 21510670]
32. Zhang BL, Li YQ, Fang CY, et al. Receptor-Mediated Cellular Uptake of Folate-Conjugated Fluorescent Nanodiamonds: A Combined Ensemble and Single-Particle Study. Small. 2009; 5(23): 2716–2721. [PubMed: 19743434]
33. Li ML, Wang JC, Schwartz JA, et al. In-vivo photoacoustic microscopy of nanoshell extravasation from solid tumor vasculature. Journal of Biomedical Optics. 2009; 14(1)
34. Paciotti GF, Myer L, Weinreich D, et al. Colloidal gold: A novel nanoparticle vector for tumor directed drug delivery. Drug Delivery. 2004; 11(3):169–183. [PubMed: 15204636]
35. Liu JB, Yu MX, Zhou C, et al. Passive Tumor Targeting of Renal-Clearable Luminescent Gold Nanoparticles: Long Tumor Retention and Fast Normal Tissue Clearance. Journal of the American Chemical Society. 2013; 135(13):4978–4981. [PubMed: 23506476]
36. Dahoumane SA, Nguyen MN, Thorel A, et al. Protein-Functionalized Hairy Diamond Nanoparticles. Langmuir. 2009; 25(17):9633–9638. [PubMed: 19634873]

37. Lim TS, Fu CC, Lee KC, et al. Fluorescence enhancement and lifetime modification of single nanodiamonds near a nanocrystalline silver surface. Physical Chemistry Chemical Physics. 2009; 11(10):1508–1514. [PubMed: 19240927]

38. Song KH, Wang LV. Deep reflection-mode photoacoustic imaging of biological tissue. Journal of Biomedical Optics. 2007; 12(6):060503. [PubMed: 18163798]

39. Cui HZ, Yang XM. In vivo imaging and treatment of solid tumor using integrated photoacoustic imaging and high intensity focused ultrasound system. Medical Physics. 2010; 37(9):4777–4781. [PubMed: 20964197]

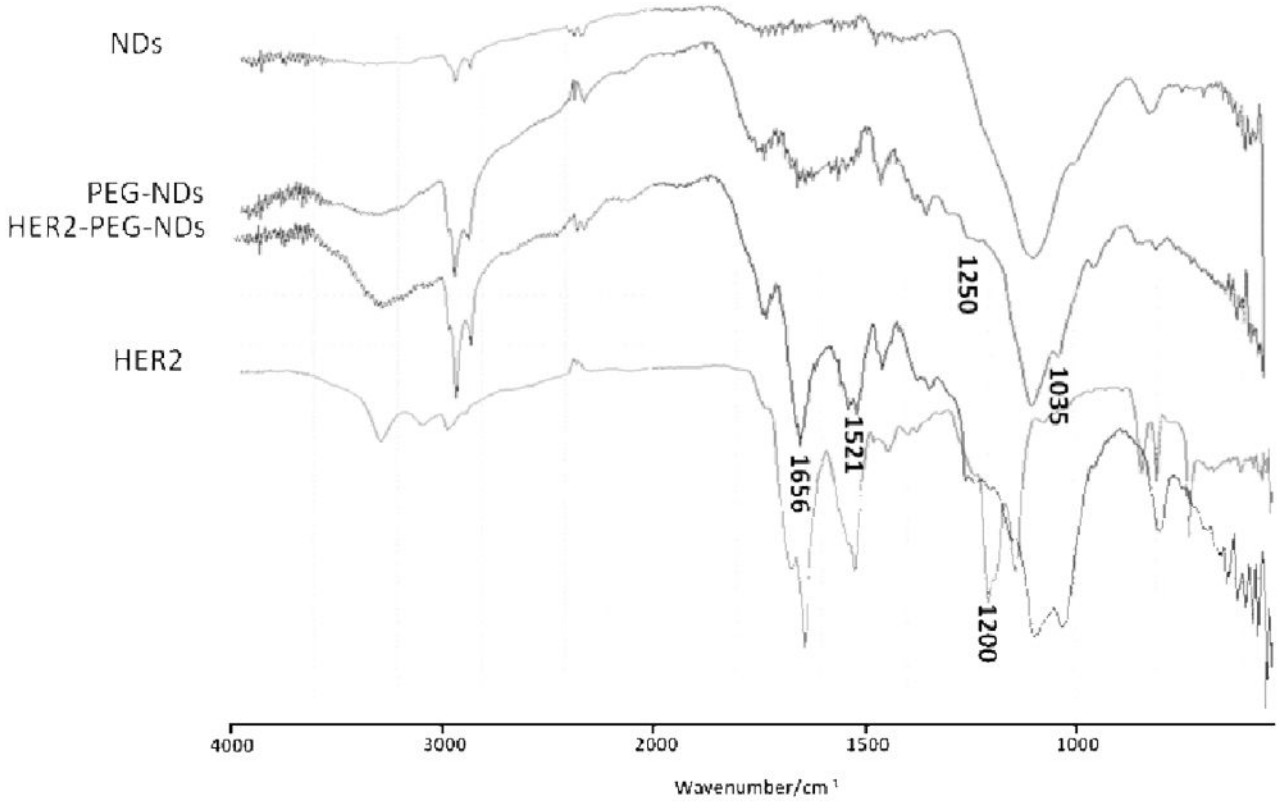

Figure 1.
Infrared spectra of ND, PEGylated NDs (PEG-NDs), HER2-PEGylated NDs (HER2-PEG-NDs) and anti-HER2 peptide.

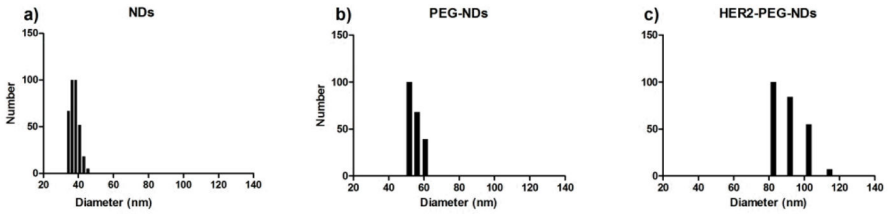

Figure 2.
Particle size distribution of (a) NDs, (b) PEG-NDs and (c) HER2-PEG-NDs.

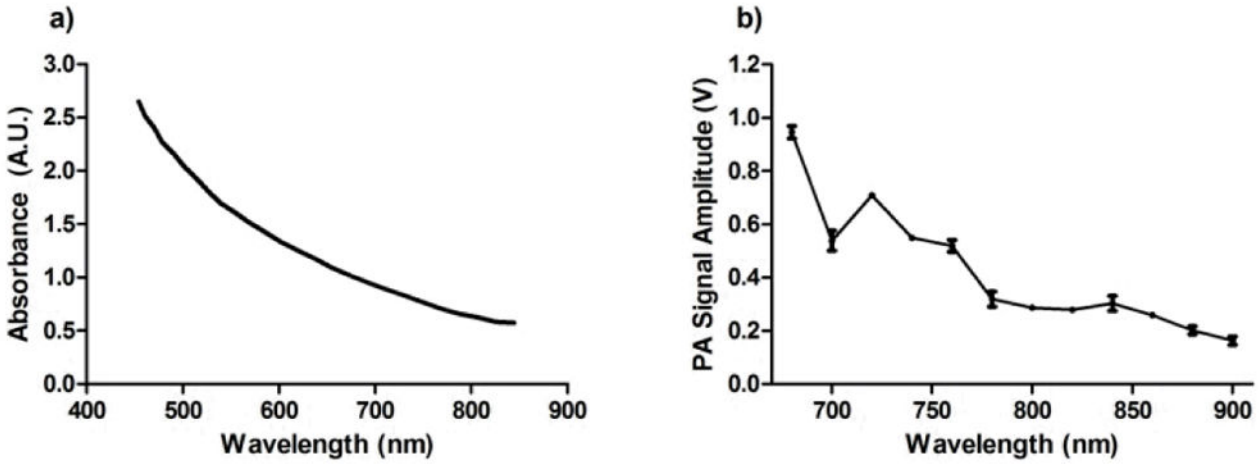

Figure 3.
Particle size distribution of (a) NDs, (b) PEG-NDs and (c) HER2-PEG-NDs.

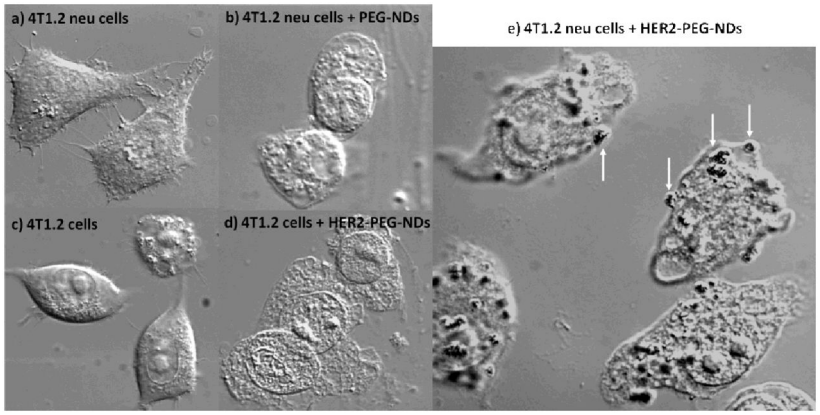

Figure 4.

Brightfield images of murine breast cancer cells. (a) Non-treated 4T1.2 neu cells, (b) 4T1.2 neu cells treated with PEG-NDs, (c) Non-treated 4T1.2 cells, (d) 4T1.2 cells treated with HER2-PEG-NDs and (e) 4T1.2 neu cells treated with HER2-PEG-NDs.

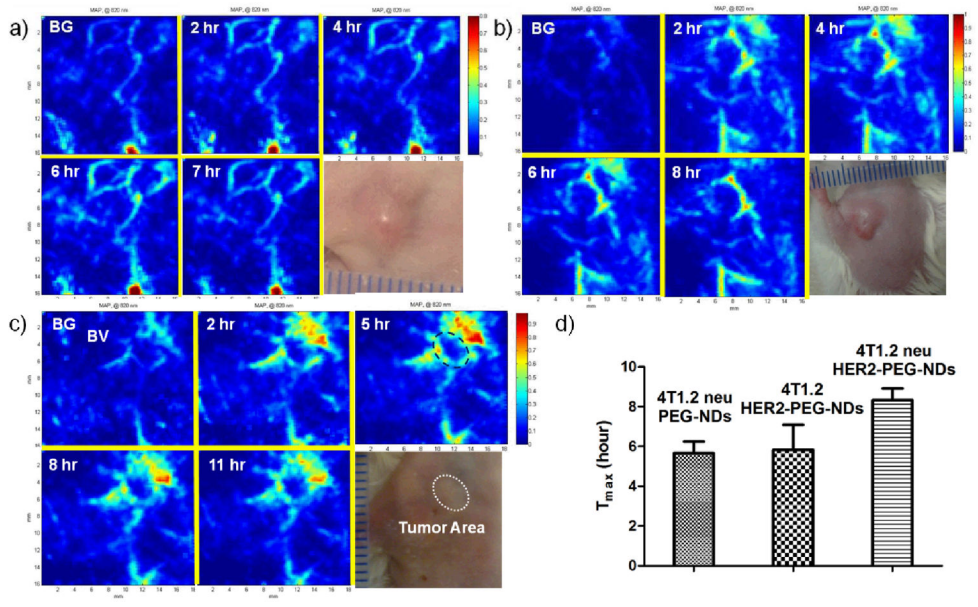

Figure 5.

PA images of ROI before and at different time points after the injection of NDs and photographs of ROI. a) 4T1.2 neu tumor model injected with PEG-NDs, (b) 4T1.2 tumor model injected with HER2-PEG-NDs, c) 4T1.2 neu tumor model injected with HER2-PEG-NDs, and (d) particle retention time in each group.

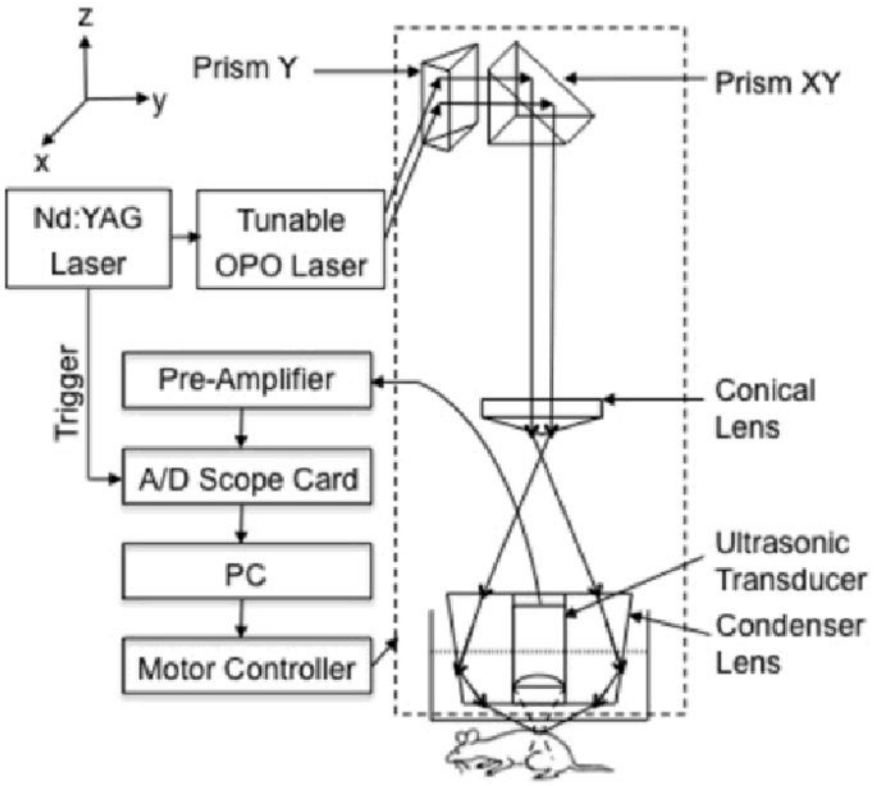

Scheme 1.
Schematic of photoacoustic imaging system.

Table 1

Measured particle sizes and zeta-potentials of NDs, PEGylated NDs and HER2 targeting peptide conjugated PEG-NDs.

Particles	Diameter (nm)	Zeta-potentials (mV)
NDs	38.3 ± 0.03	−36.49 ± 1.27
PEG-NDs	56.0 ± 0.1	−33.07 ± 1.44
HER2-PEG-NDs	92.1 ± 1.077	−22.67 ± 1.07